ELSEVIER

Imaging

THREE-DIMENSIONAL ANISOTROPY CONTRAST IMAGING OF GLIOMATOSIS CEREBRI: TWO CASE REPORTS

Takashi Inoue, M.D., Kuniaki Ogasawara, M.D., Takaaki Beppu, M.D., and Akira Ogawa, M.D.

Department of Neurosurgery, Iwate Medical University School of Medicine, Morioka, Iwate, Japan

Inoue T, Ogasawara K, Beppu T, Ogawa A. Three-dimensional anisotropy contrast imaging of gliomatosis cerebri: two case reports. Surg Neurol 2004;62:151–155.

BACKGROUND

Magnetic resonance imaging (MRI) can provide a preoperative diagnosis of gliomatosis cerebri, but the findings sometimes do not correspond with the clinical symptoms or histologic findings.

CASE DESCRIPTION

Three-dimensional anisotropy contrast (3DAC) imaging was used to assess damage to the neuronal fibers in two patients with gliomatosis cerebri who presented with only mental deterioration. Conventional MRI depicted markedly abnormal findings consisting of widespread areas of abnormally high signal intensity in the corpus callosum and in the bilateral white matter in both cases. In contrast, 3-D AC imaging showed no abnormality except for small dark areas in the corpus callosum or white matter.

CONCLUSION

3-D AC imaging provides more accurate information about damage to the neuronal fibers in cases of gliomatosis cerebri than other MRI techniques.

KEY WORDS

Gliomatosis cerebri, neuronal fiber, three-dimensional anisotropy contrast.

Gliomatosis cerebri is a rare variant of glioma characterized by diffuse proliferation of glial elements infiltrating normal nervous tissue with relative preservation of the underlying brain architecture [1,5,13]. The clinical manifestations include mental deterioration, personality change, and signs of increased intracranial pressure [4,8,14]. Disconnection syndrome may be detected in patients with infiltrating tumors involving the corpus callosum [12,17,19].

We treated 2 patients with gliomatosis cerebri who presented with only mental deterioration. Damage to the neuronal fibers was assessed using three-dimensional (3-D) anisotropy contrast (3DAC) imaging.

CASE REPORTS

PATIENT 1

A 48-year-old woman in good health suffered generalized tonic convulsion. On admission, general physical examination found no abnormalities. Neurologic examination identified no motor weakness, no sensory deficit, and neither apraxia nor agnosia. Testing of cognitive function demonstrated mental deterioration: verbal intelligence quotient (IQ) was 60 points and performance IQ was 58 points on the Wechsler Adult Intelligence Scale-Revised (WAIS-R) [21].

Magnetic resonance imaging (MRI) was performed with a Signa VH/i 3.0 T (General Electric Systems, Milwaukee, WI). Short inversion time inversion recovery (STIR) sequence was used for T2-weighted imaging with the following parameters: repetition time (TR) 5000 ms, echo time (TE) 25 ms, inversion time 140 ms, matrix 512 × 384, field of view (FOV) 240 mm, and 6 mm slice thickness. Diffusion-weighted (DW) imaging with motion providing gradients applied in three directions was also performed to investigate the neuronal fibers using the following parameters: TR 6000 ms, TE 80 ms, matrix 256 × 260, FOV 240 mm, 6 mm slice thickness, and b value 800 s/mm^2. The DW images were transferred to a personal computer and 3-D AC images were generated to visualize the directional-

Address reprint requests to: Takashi Inoue, M.D., Department of Neurosurgery, Iwate Medical University School of Medicine, 19-1 Uchimaru, Morioka, Iwate 020-8505, Japan.

Received August 7, 2002; accepted August 21, 2003.

360 Park Avenue South, New York, NY 10010-1710

0090-3019/03/$–see front matter
doi:10.1016/j.surneu.2003.08.031

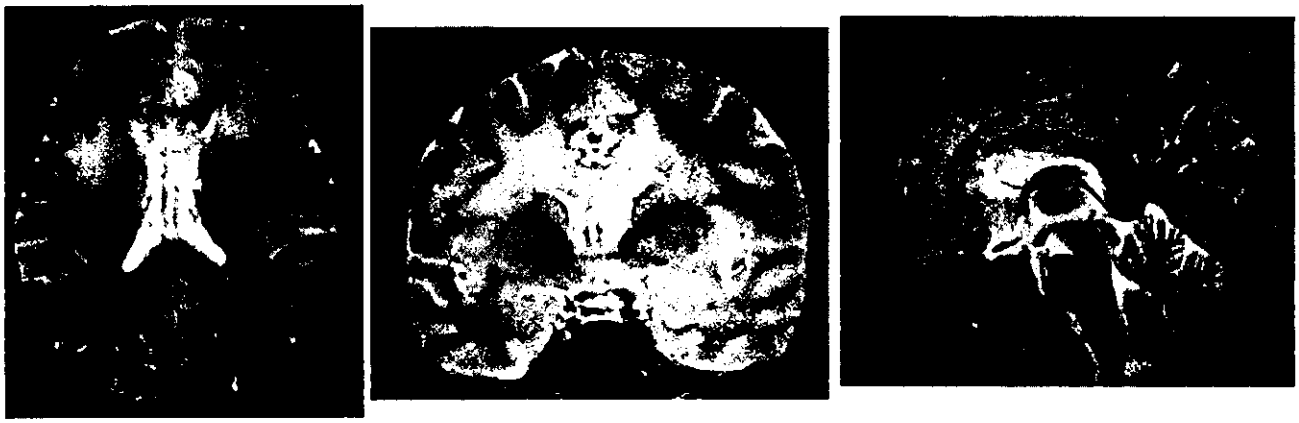

1 Axial (*left*), coronal (*center*), and sagittal (*right*) short inversion time inversion recovery images showing diffuse high-intensity lesions. Tumor invasion was apparently present in the enlarged corpus callosum, indicating a space-occupying lesion.

ity and damage in the neuronal fibers [10,16]. The STIR images depicted widespread areas of abnormally high signal intensity in the corpus callosum and in the white matter of the bilateral frontal and parietal lobes (Figure 1). In contrast, the 3DAC images showed no abnormality except for small dark areas in the corpus callosum (Figure 2).

Brain biopsy was performed by a stereotactic technique. Histologic examination of the specimens obtained from the corpus callosum showed diffuse glial infiltration. The majority of cells were spindle shaped with moderately differentiated neoplasticity and contained abnormally swollen nuclei (Figure 3). The histologic diagnosis was fibrillary astrocytoma.

PATIENT 2

A 68-year-old woman was transferred to our hospital after presenting with complaints of headaches. Computed tomography of the head revealed diffuse areas of abnormally low density. On admission, general physical examination found no abnormalities. Neurologic examination identified no motor weakness, no sensory deficit, and neither apraxia nor agnosia. Testing of cognitive function demonstrated mental deterioration: verbal IQ was 86 points and performance IQ was 61 points on the WAIS-R.

The STIR images showed widespread areas of abnormally high signal intensity in the splenium

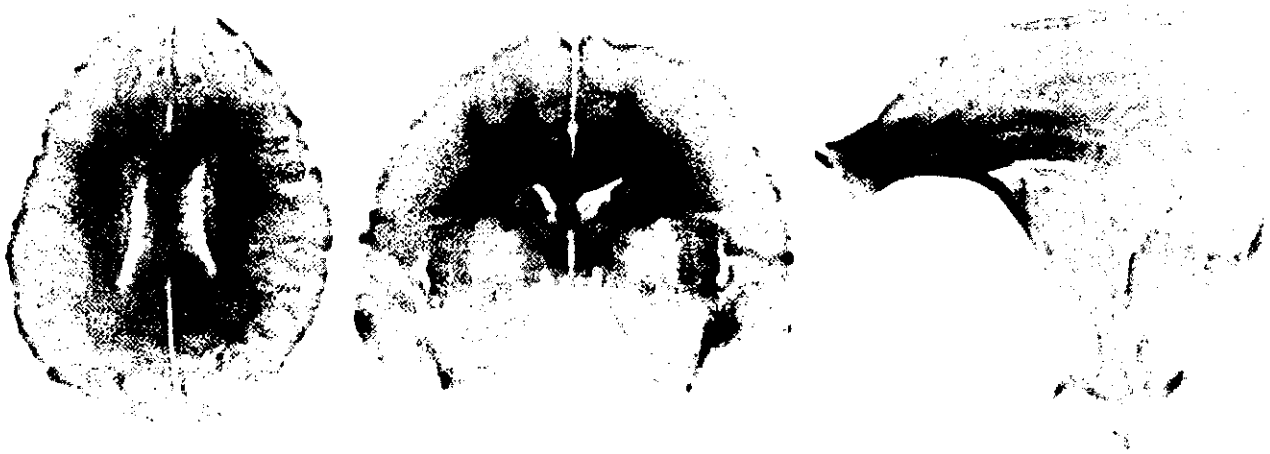

2 Axial (*left*), coronal (*center*), and sagittal (*right*) three-dimensional anisotropy contrast images. Neuronal fibers running in the superior-inferior, left-right, or anterior-posterior directions are assigned red, green, or blue, respectively. Mixed colors indicate oblique orientation of the neuronal fibers. The damaged fibers appear as dark areas, whereas the green area indicates that the neuronal fibers were running left to right or right to left in the corpus callosum. Image distortion was caused by a susceptibility artifact in the sagittal image.

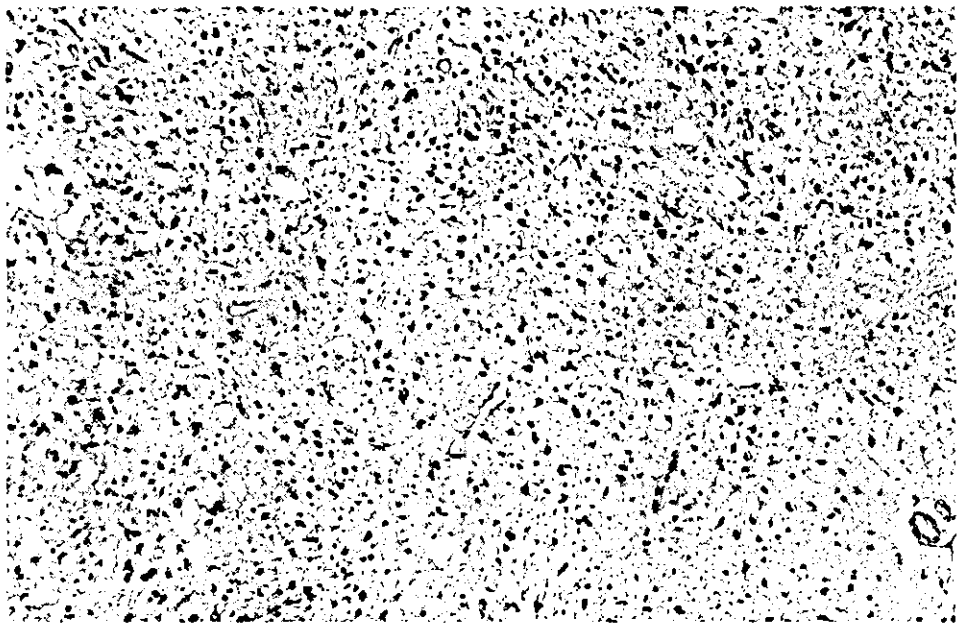

3 Photomicrograph of the specimen from the corpus callosum revealing increased numbers of glial cells (H&E; original magnification, × 100).

and in the white matter of the bilateral occipital and frontal lobes (Figure 4 left). In contrast, the 3DAC images showed no abnormality except for the dark areas in the occipital lobe (Figure 4 right).

Brain biopsy was performed by a stereotactic technique. The histologic diagnosis was fibrillary astrocytoma.

Discussion

MRI can confirm the preoperative diagnosis of gliomatosis cerebri [5–7,15,18], because T2- or proton density-weighted MRI demonstrates the lesions as abnormally high intensity areas. However, histologic examination shows that abnormal glial cells

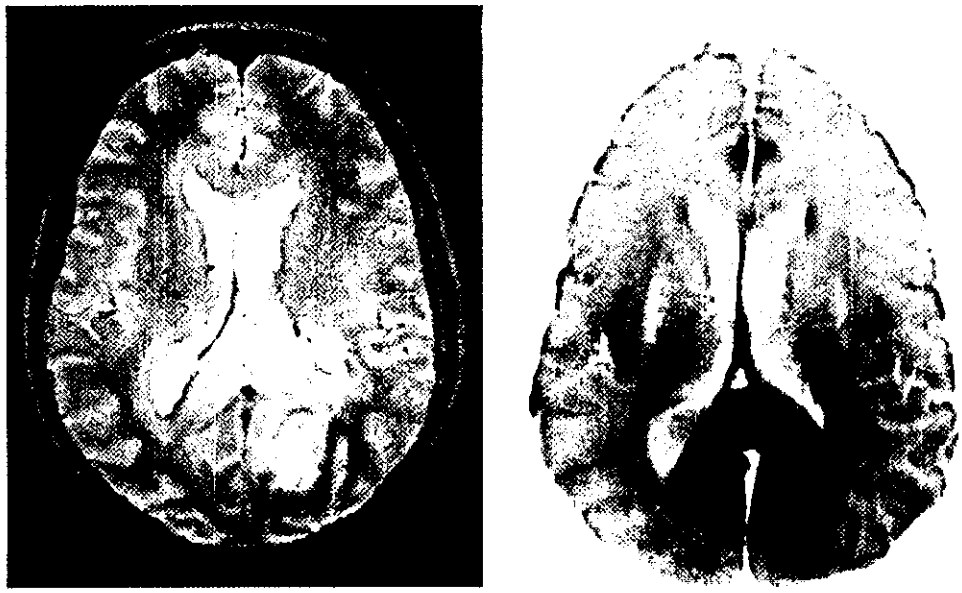

4 *Left:* Short inversion time inversion recovery image showing diffuse high-intensity lesions. Tumor invasion was apparently present in the enlarged corpus callosum, indicating a space-occupying lesion. *Right:* Three-dimensional anisotropy contrast image. Neuronal fibers running in the superior-inferior, left-right, or anterior-posterior directions are assigned red, green, or blue, respectively. Mixed colors indicate oblique orientation of the neuronal fibers. The corpus callosum appears as blue and green, which indicates that the neuronal fibers were not destroyed.

infiltrate the white matter along the anatomic pathways without destruction of the normal architecture [3,6,22]. The primary manifestations are not focal neurologic deficits as expected based on the findings of MRI but mental changes and increased intracranial pressure as expected based on the histologic features [1,2,14].

3DAC imaging is an established method to visualize directionality and damage in the neuronal fibers [9–11,20]. 3DAC imaging is useful to investigate the pathologic involvement of the pyramidal tract in patients with brain tumors [10]. In the present 2 cases, STIR imaging showed distinct abnormally high intensity areas in the corpus callosum and in the bilateral white matter, whereas 3DAC imaging showed no signal abnormality except for small dark areas in the corpus callosum or white matter. Clinically, both patients presented with no neurologic symptoms other than mental deterioration. Histologically, the specimens obtained from the corpus callosum showed existence of tumor cells. Although 3DAC imaging has some limitation to estimate the tumor existence, these findings suggest that 3DAC imaging provides more accurate information about damage to the neuronal fibers in patients with gliomatosis cerebri than other MRI methods.

This work was supported in part by Grants-in-Aid for Advanced Medical Science Research from the Ministry of Education, Culture, Sports, Science, and Technology, Japan.

REFERENCES

1. Artigas J, Cervos-Navarro J, Iglesias JR, Ebhardt G. Gliomatosis cerebri: clinical and histological findings. Clin Neuropathol 1985;4:135–48.
2. Couch JR, Weiss SA. Gliomatosis cerebri. Report of four cases and review of the literature. Neurology 1974;24:504–11.
3. Cummings TJ, Hulette CM, Longee DC, Bottom KS, McLendon RE, Chu CT. Gliomatosis cerebri: cytologic and autopsy findings in a case involving the entire neuraxis. Clin Neuropathol 1999;18:190–7.
4. Dickson DW, Horoupian DS, Thal LJ, Lantos G. Gliomatosis cerebri presenting with hydrocephalus and dementia. AJNR Am J Neuroradiol 1988;9:200–2.
5. Felsberg GJ, Silver SA, Brown MT, Tien RD. Radiologic-pathologic correlation. Gliomatosis cerebri. AJNR Am J Neuroradiol 1994;15:1745–53.
6. Freund M, Hahnel S, Sommer C, et al. CT and MRI findings in gliomatosis cerebri: a neuroradiologic and neuropathologic review of diffuse infiltrating brain neoplasms. Eur Radiol 2001;11:309–16.
7. Galatioto S, Marafioti T, Cavallari V, Batolo D. Gliomatosis cerebri. Clinical, neuropathological, immunohistochemical and morphometric studies. Zentralbl Pathol 1993;139:261–7.
8. Giovagnoli AR, Strada L, Pollo B, Boiardi A. Gliomatosis cerebri. Report of a case with isolated amnesic disorders. Ital J Neurol Sci 1992;13:503–6.
9. Igarashi H, Katayama Y, Tsuganezawa T, Yamamuro M, Terashi A, Owan C. Three-dimensional anisotropy contrast (3DAC) magnetic resonance imaging of the human brain: application to assess Wallerian degeneration. Intern Med 1998;37:662–8.
10. Inoue T, Shimizu H, Yoshimoto T. Imaging the pyramidal tract in patients with brain tumors. Clin Neurol Neurosurg 1999;101:4–10.
11. Inoue T, Shimizu H, Yoshimoto T, Kabasawa H. Spatial functional distribution in the corticospinal tract at the corona radiata: a three-dimensional anisotropy contrast study. Neurol Med Chir (Tokyo) 2001;41: 293–9.
12. Jinkins JR. The MR equivalents of cerebral hemispheric disconnection: a telencephalic commissuropathy. Comput Med Imaging Graph 1991;15:323–31.
13. Kannuki S, Hirose T, Horiguchi H, Kageji T, Nagahiro S. Gliomatosis cerebri with secondary glioblastoma formation: report of two cases. Brain Tumor Pathol 1998;15:111–6.
14. Kannuki S, Hondo H, Ii K, Hirose T, Matsumoto K. Gliomatosis cerebri with good prognosis. Brain Tumor Pathol 1997;14:53–7.
15. Koslow SA, Claassen D, Hirsch WL, Jungreis CA. Gliomatosis cerebri: a case report with autopsy correlation. Neuroradiology 1992;34:331–3.
16. Nakada T, Matsuzawa H, Kwee IL. Magnetic resonance axonography of the rat spinal cord. Neuroreport 1994;5:2053–6.
17. Plowman PN, Saunders CA, Maisey MN. Gliomatosis cerebri: disconnection of the cortical grey matter, demonstrated on PET scan. Br J Neurosurg 1998;12: 240–4.
18. Rippe DJ, Boyko OB, Fuller GN, Friedman HS, Oakes WJ, Schold SC. Gadopentetate-dimeglumine-enhanced MR imaging of gliomatosis cerebri: appearance mimicking leptomeningeal tumor dissemination. AJNR Am J Neuroradiol 1990;11:800–1.
19. Sidtis JJ, Sadler AE, Nass RD. Double disconnection effects resulting from infiltrating tumors. Neuropsychologia 1989;27:1415–20.
20. Watanabe T, Honda Y, Fujii Y, Koyama M, Matsuzawa H, Tanaka R. Three-dimensional anisotropy contrast magnetic resonance axonography to predict the prognosis for motor function in patients suffering from stroke. J Neurosurg 2001;94:955–60.
21. Wechsler D. Manual for the Wechsler Adult Intelligence Scale-Revised. New York: The Psychological Corporation, 1981.
22. Yanaka K, Kamezaki T, Kobayashi E, Matsueda K, Yoshii Y, Nose T. MR imaging of diffuse glioma. AJNR Am J Neuroradiol 1992;13:349–51.

COMMENTARY

The authors describe the use of 3-D anisotropy contrast (3 DAC) MRI to assess damage to the neuronal fibers in 2 patients with gliomatosis cerebri.

The useful use of 3 DAC highlights the trend toward 3-D MR axonography. Many reports have been published showing the usefulness of 3 DAC MRI to assess wallerian degeneration, involvement of py-

ramidal tract in patients with brain tumor, and demyelinating disease. The authors' report on 2 patients with gliomatosis cerebri, a rare disease, is another interesting application to study the gliomatosis cerebri. Their finding on 3 DAC is very interesting. However, does this justify believing there is no tumor along the tract? The diagnostic accuracy of 3 DAC MRI in their cases has not been studied by biopsy of areas, which were dark on 3 DAC MRI. It is an important imaging technique; however, its sensitivity is certainly less than perfect.

Clinical cranial MRI examinations include spin-echo T_1-weighted (T_1W), spin-echo T_2-weighted (T_2W) gradient echo pulse sequence, and fluid attenuation inversion recovery (FLAIR) pulse sequence. T_2W and FLAIR images generally depict more pathologic lesions than do spin-echo T_1W MR images. Gradient echo images are very useful to detect blood by-products, as well as calcification. Diffusion-weighted MRI (DWI) is widely used for the detection of acute ischemic stroke [1]. The contrast on a diffusion-weighted image of the brain is affected by the direction of white matter fiber pathways [2] to determine the direction and corresponding diffusivity of white fibers. The diffusion tensor imaging that characterizes anisotropic diffusion in 3D has to be performed [3]. Several methods that utilize diffusion anisotropy have been developed to depict the white matter fiber pathways [4]. Some of these methods use colors and the appearance of color image may depend on the choice of the computer display [2,5]. These techniques provide added information regarding the direction of white matter fibers so that structures that are indistinct on the spin-echo T_2W image may be delineated.

The white matter fiber pathways, in particular corpus callosum optic radiation, internal capsule and superior longitudinal fasciculus can be clearly identified. In addition, superposition of a spin-echo T2W MRI and a color-coded image, derived from three orthogonal diffusion-weighted images could show white matter tract architecture to further assess brain pathology.

Mahmood F. Mafee, M.D.
Department of Radiology
University of Illinois at Chicago
Chicago, Illinois

REFERENCES

1. Burdette JH, Elster AD, Ricci PE. Acute cerebral infarction: quantification of spin-density and T2 shine-through phenomena on diffusion-weighted MR images. Radiology 1999;212:333–9.
2. Tamura H, Takahashi S, Kurihara N, Yamada S, Hatazawa J, Okudera T. Practical visualization of internal structure of white matter for image interpretation: staining a spin-echo T2-weighted image with three echo-planar diffusion-weighted images. AJNR, Am J Neuroradiol 2003;24:401–9.
3. Shrager RJ, Basser PJ. Anisotropically weighted MRI. Magn Reson Med 1998;40:160–5.
4. Jones DK, Simmons A, Williams SC, Horsfield MA. Non-invasive assessment of axonal fiber connectivity in the human brain via diffusion tensor MRI. Magn Reson Med 1999;42:37–41.
5. Pajevic S, Pierpaoli C. Color schemes to represent the orientation of anisotropic tissues from diffusion tensor data: application to white matter fiber tract mapping in the human brain. Magn Reson Med 1999;42:526–40.

Available online at www.sciencedirect.com

SCIENCE DIRECT

Surgical Neurology 63 (2005) 56–61

SURGICAL NEUROLOGY

www.surgicalneurology-online.com

Imaging

Fractional anisotropy value by diffusion tensor magnetic resonance imaging as a predictor of cell density and proliferation activity of glioblastomas

Takaaki Beppu, MD[a,*], Takashi Inoue, MD[a], Yuji Shibata, PhD[b], Noriyuki Yamada, PhD[c], Akira Kurose, MD[b], Kuniaki Ogasawara, MD[a], Akira Ogawa, MD[a], Hiroyuki Kabasawa, DEng[d]

Departments of [a]Neurosurgery, [b]First Department of Pathology, and [c]Clinical Pathology, Iwate Medical University, Morioka 020-8505, Japan

[d]GE Yokogawa Medical Systems, Tokyo, Japan

Received 4 March 2003; accepted 12 February 2004

Abstract

Background: In vivo, water diffusion displays directionality due to presence of complex microstructural barriers in tissue. The extent of directionality of water diffusion can be expressed as a fractional anisotropy (FA) value using diffusion tensor magnetic resonance imaging (DTI). The FA value has been suggested as an indicator of the cell density of astrocytic tumors. The aim of the present study was to confirm beyond doubt that FA values indicate cell density even when limited in glioblastomas and to determine whether the FA value of a given patient predicts proliferation activity in the individual glioblastoma.

Methods: We performed DTI in 19 patients with glioblastoma and measured the FA values of tumor and normal brain regions prior to computed tomography–guided stereotactic biopsy. Differences in mean FA value between normal brain regions and glioblastoma lesion were compared. Cell density and MIB-1 indices were examined using tumor specimens obtained from biopsies. Correlation among FA values, cell density, and MIB-1 indices was also evaluated.

Results: The mean FA value significantly differed between normal brain regions and glioblastoma lesions. Positive correlation was observed between FA value and cell density ($r = 0.73$, $P < 0.05$) and between FA value and MIB-1 index ($r = 0.80$, $P < 0.05$).

Conclusions: Our results suggest that the FA value of glioblastoma as determined by DTI prior to surgery is a good predictor of cell density and, consequently, proliferation activity.

Keywords: Cell density; Diffusion tensor magnetic resonance imaging; Fractional anisotropy; Glioblastoma; Proliferation

1. Introduction

Essentially, the diffusion of water molecules displays microscopic random (Brownian) translational motion, and under these conditions, the molecular mobility of water is the same in all directions. In vivo, water diffusion takes on an abnormal motion due to hindrance by the presence of complex microstructural barriers in tissue, such as white matter tracts, cell membranes, and/or capillary vessels, and consequently the change in magnitude and directionality of water diffusion arises in a 3-dimensional space [2]. This directional variation is termed diffusion anisotropy. Diffusion tensor magnetic resonance imaging (DTI) provides quantitative information about the magnitude and directionality of water diffusion along a vector in a 3-dimensional space [4,6,17,26]. Evaluation of directionality of water diffusion using DTI has recently become available for visualization of cerebral fiber tracts [26] and demonstration of substantial differences among the various lesions of multiple sclerosis [1,7,8,24]. In DTI, a set of orthogonal vectors known as eigenvectors, which define the orientation of the principal axes of a diffusion ellipsoid in space, are

* Corresponding author. Tel.: +81 196 51 5111x6603; fax: +81 196 25 8799.

E-mail address: tbeppu@iwate-med.ac.jp (T. Beppu).

0090-3019/$ – see front matter © 2005 Elsevier Inc. All rights reserved.
doi:10.1016/j.surneu.2004.02.034

calculated from the diffusion tensor. The length of each vector is represented by corresponding eigenvalues. The fractional anisotropy (FA) is derived from eigenvectors for quantification of anisotropy. A FA value is calculated using the following formula based on eigenvalues in the diffusion tensor [2,18]:

$$FA = \sqrt{\frac{3}{2}} \frac{\sqrt{(\lambda_1 - \langle D \rangle)^2 + (\lambda_2 - \langle D \rangle)^2 + (\lambda_3 - \langle D \rangle)^2}}{\sqrt{\lambda_1^2 + \lambda_2^2 + \lambda_3^2}} \cdots \quad (1)$$

$$\langle D \rangle = \frac{1}{3}(\lambda_1 + \lambda_2 + \lambda_3) \cdots \quad (2)$$

where λ_1, λ_2, and λ_3 are the largest, intermediate, and smallest eigenvalues, respectively, of the diffusion tensor. The FA is expressed as a numerical value between 0 and 1 without a unit. A higher FA value implies a greater degree of anisotropic motion of water molecules.

Presurgical knowledge of the cell density and proliferation potential of the tumor tissue would have prognostic significance and help to elucidate the histologic characteristics in individual patients with astrocytic tumors. Water diffusion has been suggested to be affected by tumor cellularity in gliomas [22]. Our preliminary study suggested a correlation between the FA value and the tumor cell density or malignancy grades in astrocytic tumors [3], which led to the presumption that FA values also correlate with the cell proliferation activity of astrocytic tumors. To date, whether FA can act as an indicator of cell proliferation in astrocytic tumors is unknown. The quantitative estimation of cell density or proliferation is largely complicated by widely distributed values of differently graded astrocytic tumors when a study involves a group of mixed, differently graded tumors. To confirm whether FA values indicate cell density and proliferation activity of an astrocytic tumor group limited to 1 type, we examined the relationship among FA value, tumor cell density, and MIB-1 index, which is widely used as a quantitative information of cell proliferation [10,12,19,25] in glioblastomas alone.

2. Materials and methods

2.1. Patient population

The study protocol was approved by the Ethics Committee of Iwate Medical University (Morioka, Japan). The patients recruited to this study were admitted to the Department of Neurosurgery, Iwate Medical University, between September 2000 and December 2002. Entry criteria for this study were as follows: (A) adult patients who were diagnosed with supratentorial glioblastoma; (B) patients whose tumor was primarily in the cerebral white matter, except for the basal ganglia, corpus callosum, ventricle, and brain stem; (C) patients who received routine magnetic resonance imaging (MRI) and DTI within the 2 weeks prior to computed tomography–guided stereotactic biopsy; and (D) informed written consent to participate. Diagnosis was based on the histologic features of specimens obtained from a stereotactic biopsy according to the World Health Organization classification [13]. A total of 19 patients (11 males and 8 females; mean age, 58.9 years; age range, 28-77 years) participated. The main tumor sites were the frontal lobe in 6 patients, parietal lobe in 7, temporal lobe in 5, and occipital lobe in 1.

2.2. Measurement of FA value

All routine MRI and DTI scans were performed using a 3.0 T MRI system (Signa VH/I, GE Medical Systems, Milwaukee, WI) with a standard head coil. A spin echo–type echo planar imaging sequence with diffusion gradients applied in 6 directions was used for the diffusion tensor imaging: repetition time 10,000 ms, echo time 84 ms, matrix 256 × 260, field of view 240 mm^2, 6 mm thickness, 2 mm gap, b factors 800 s/mm^2. All patients also underwent conventional spin echo T1- and T2-weighted imaging prior to DTI and T1-weighted imaging with contrast medium after DTI. All image analysis after processing was performed on a scanner console using a subprogram of the Functool image analysis software (GE Medical Systems, Buc, France) modified by one of the investigators (HK).

The region of interest (ROI) was determined on a slice showing maximal tumor size in T1-weighted imaging with contrast medium, because the tumors of all patients were detected as enhancing lesions. Where possible, the ROI was placed at the enhancing central region of the tumor. If central necrosis was evident, the ROI was placed on a ring-enhancing region of the tumor containing more metabolically active sites than the central region (Fig. 1A). The ROI was also placed in subcortical normal white matter (NWM) where no abnormalities on T2-weighted MRI were detected. When the tumor was sited in the frontal lobe or anterior half of the temporal lobe, the ROI was placed in subcortical white matter of the contralateral occipital lobe. On the other hand, the ROI was placed in subcortical white matter of the contralateral frontal lobe when the tumor was situated in the parietal lobe, the occipital lobe, or the posterior half of the temporal lobe. If the tumor was not in or had not infiltrated into the corpus callosum on T2-weighted MRI, the ROI was placed at the genu or splenium of the corpus callosum. When the tumor was sited in the frontal lobe or anterior half of the temporal lobe, the ROI was placed in the splenium, whereas the ROI was placed in the genu when the tumor was situated in the parietal lobe, the occipital lobe, or the posterior half of the temporal lobe. ROIs were automatically transferred onto the coregistered FA maps constructed from DTI (Fig. 1B, C). The FA values were then calculated for each patient using the modified Functool image analysis software. The FA value was identified as a mean of values derived for every pixel in a

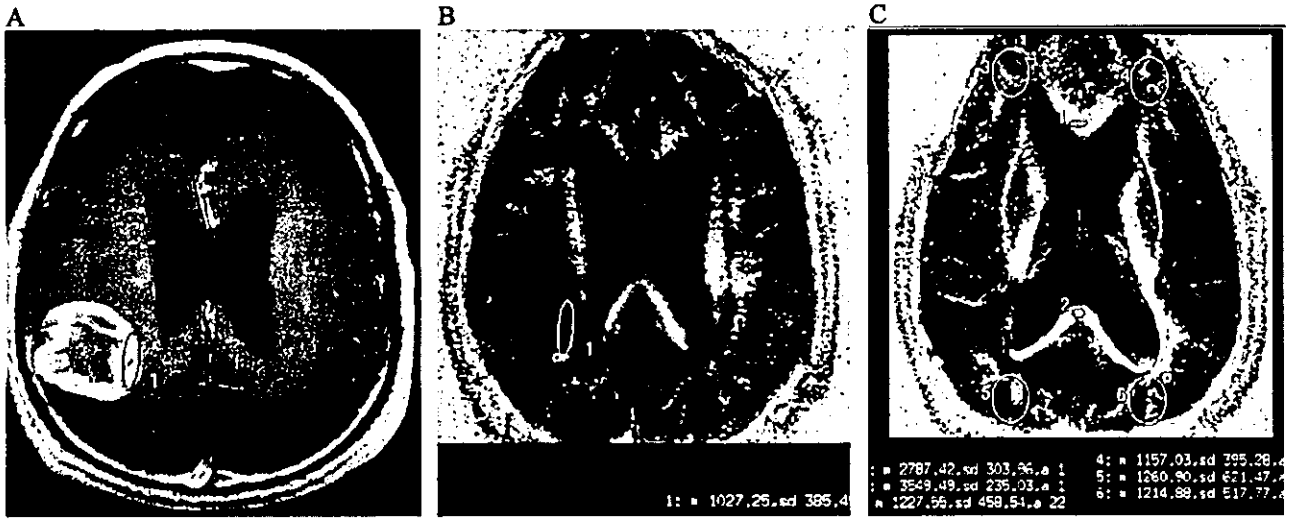

Fig. 1. Locations of ROI in a patient with glioblastoma of the right parietal lobe. A, Gadolinium-enhanced T1-weighted MR image. Circle, ROI within a ring-enhancing lesion of the tumor. B, The coregistered FA maps from DTI. The ROI that was determined from the gadolinium-enhanced T1-weighted MR image was transferred onto a FA map. C, FA map for NWM. Because the tumor was situated in the parietal lobe, only FA values in ROIs of the contralateral frontal lobe (No 4) and the genu (No 1) were accepted.

given ROI. All MRI and DTI procedures were performed by 1 investigator (TI).

2.3. Tumor tissue specimens

In all patients, the tumor tissue specimens were obtained by computed tomography–guided stereotactic biopsy targeted to the intratumoral area corresponding exactly to the ROI within which the FA value was measured. For patients who underwent tumor resection with a large craniotomy, stereotactic biopsy was performed prior to tumor resection. In these patients, a silicon tube was left in the intracerebral trajectory made by the biopsy and was then used as a guide for tumor localization during tumor resection.

After biopsy, specimens were immediately fixed in 30% formalin for 24 hours at room temperature and then embedded in paraffin. Each paraffin block was cut into 6-μm-thick serial sections that were used for hematoxylin and eosin staining and Ki-67 immunohistochemical staining. Cell density was identified as the mean of tumor cell numbers in hematoxylin and eosin–stained preparations in 10 fields of a square 25 μm per side under 200 × magnification. Ki-67 was immunohistochemically detected using anti-Ki-67 monoclonal antibody (MIB-1, DAKO, Copenhagen, Denmark) diluted 1:50 and was stained by the modified avidin-biotin-peroxidase complex method [11]. Prior to Ki-67 immunohistochemical staining, sections were treated in an autoclave at 121°C for 15 minutes. The percentage of stained positive cells in approximately 1000 cells, except for inflammatory cells and vascular cells, under a light microscope (200 ×) was defined as the MIB-1 index for that patient. All histologic analyses were performed by 3 investigators (YS, NY, and AK) with no prior knowledge of the patient data.

2.4. Statistical analysis

Mean FA values of subcortical NWM, normal corpus callosum, and glioblastoma tissue were calculated and then compared statistically using 1-factor ANOVA. Correlation among FA values, cell density, and MIB-1 indices of glioblastoma tissues was analyzed statistically using Pearson's correlation coefficient. Statistical significance was established at the $P < 0.05$ level.

3. Results

The mean FA values of the corpus callosum (the genu in 9 patients and the splenium in 10 patients), subcortical white

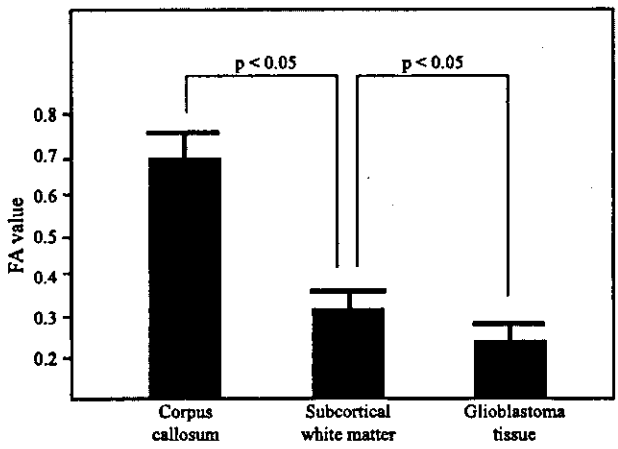

Fig. 2. Mean FA values of regions in NWM and glioblastoma. Significant differences in mean FA values were observed between the corpus callosum, subcortical white matter and glioblastoma lesion.

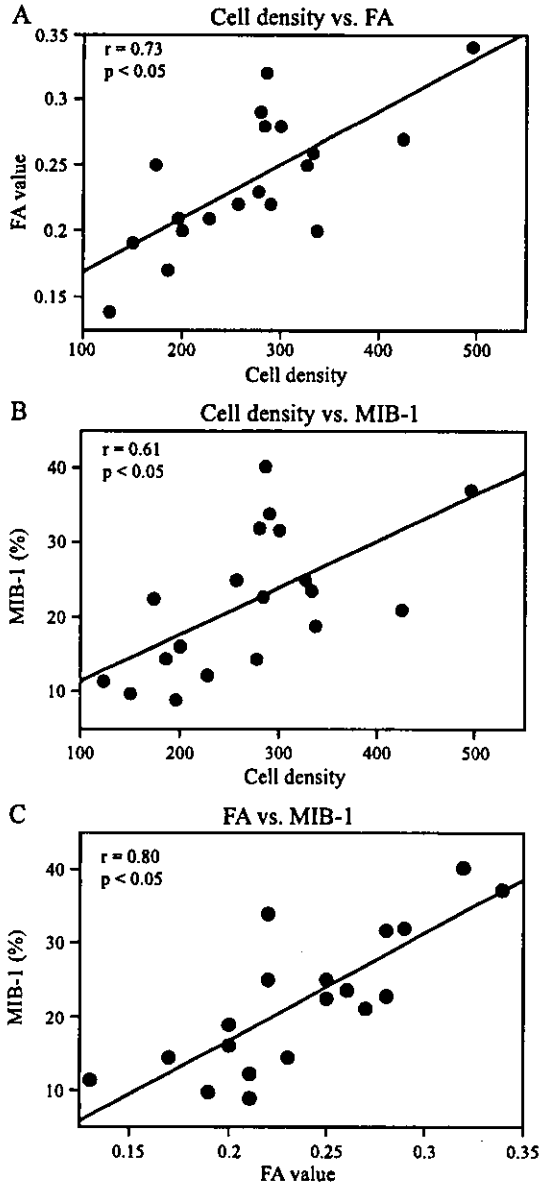

Fig. 3. Correlation between FA value and cell density (A), between cell density and MIB-1 index (B), and between FA value and MIB-1 index (C) in all patients. Strong correlation was observed between FA value and cell density (A) and between FA value and MIB-1 index (C), whereas correlation between cell density and MIB-1 index was moderate (B).

matter (the frontal lobe in 9 patients and the occipital lobe in 10 patients), and glioblastoma lesion were 0.70 ± 0.05, 0.32 ± 0.04, and 0.24 ± 0.05, respectively. The mean FA values were significant different among the corpus callosum, subcortical white matter, and glioblastoma tissue ($P < 0.05$; Fig. 2).

In glioblastoma lesions, the mean values of cell density and MIB-1 index were 270 ± 93% and 21.6 ± 10.0%, respectively. Strong correlation was observed between FA value and cell density ($r = 0.73$, $P < 0.05$) and between FA value and MIB-1 index ($r = 0.80$, $P < 0.05$; Fig. 3A, C), whereas there was moderate correlation between cell density and MIB-1 index ($r = 0.61$, $P < 0.05$; Fig. 3B).

4. Discussion

Normal white matter shows strong directionality of water diffusion and, consequently, a high FA value, because the water diffusion parallel to the white matter tracts is less restricted than the water diffusion perpendicular to them [26]. Although limited information is available for the subcortical NWM and corpus callosum, FA values are 0.2 to 0.6 in the frontal lobe [7,8,21,24,28] and 0.6 to 0.8 in the corpus callosum [1,7,8,16,21]. The FA values in the present study for the subcortical NWM and corpus callosum were similar to those reports (Fig. 2), confirming the reliability of the FA values obtained here. On the other hand, the FA values of glioblastoma tissue have been reported to be lower than those of NWM [20], which is consistent with our result. When astrocytic tumors grow in white matter, almost all normal fiber and cell structures are destroyed by the tumor nidus or displaced and separated to surround the tumor nidus [27]. One possible explanation for the lower mean FA values of the tumor core than NWM is that destruction or displacement of normal fibers induces a decrease in the directionality of water diffusion and a relative decrease in FA value [3,20].

FA value is thought to be largely affected by tumor cell density in glioma tissue [20]. Our preliminary study reported that higher anaplastic grade and higher cell density increased the FA value of differently graded gliomas [3]. The present study indicated that FA values strongly correlated with cell density even when the analysis was limited to glioblastomas alone (Fig. 3A). We hypothesized that the FA value of astrocytic tumor tissue is determined by a balance between factors decreasing the degree of the directionality of water diffusion, such as fiber destruction or displacement, and factors increasing it, such as high cell density and/or vascularity [3]. Even in a study group limited to glioblastomas, cell density rather than normal fiber tracts would predominantly affect FA value, as normal fibers are completely destroyed or displaced to around the tumor core. In the present study, FA value strongly correlated with MIB-1 index (Fig. 3C). This finding could be arrived by syllogism (ie, correlation between FA value and cell density and between cell density and MIB-1 index) and allows the assumption of correlation between FA value and MIB-1 index. The correlation between FA value and MIB-1 index suggests that the FA value predicts not only cell density but also proliferation activity in glioblastomas. Although there is general consensus that MIB-1 index does not allow a prognosis in individual patients with glioblastoma [13], we believe that prediction of proliferation activity prior to surgery would be helpful for the diagnosis and characterization of glioblastomas.

Why FA value, which is an indicator of directionality of water diffusion, correlates strongly with cell density in glioblastoma tissue is unclear. Using diffusion-weighted MRI, evaluations of water diffusion in gliomas or the other

brain tumors have been documented previously [4,5,9,14, 15,22,23]. All authors reported that the value of the apparent diffusion coefficient, which is an indicator of the magnitude of water diffusion, decreased with tumor cell density. The apparent diffusion coefficient values negatively correlated to the cell density in both glioblastomas and diffuse astrocytomas [14]. Furthermore, low apparent diffusion coefficient value in gliomas reflects a decreased volume of extracellular space, which accelerates water diffusion due to encroachment by tumor cells, and/or an increased intracellular viscosity [5,22]. Similarly, we speculate that 1 possible reason for the correlation between FA value and cell density is that an increased amount of cellular membranes and intracellular viscosity, as well as relatively decreased extracellular space in glioblastoma tissue, also induces an increase in the extent of directionality of water diffusion within each pixel of DTI, resulting in a relative increase in FA value.

The present study possesses some limitations regarding interpretation of the FA values. First, how structural factors other than cell density (eg, vascularity, edema, microcysts, tumor cell size, bipolar processes of neoplastic cells, and velocity of flowing blood in capillaries) affect the directionality of water diffusion and alter FA values was not explored. Although the present results suggest that primarily cell density affects FA value, these other factors may also affect it to some small extent. This issue is a matter for future analysis. Second, the present results do not apply to the invading lesion around a tumor nidus. Within such lesions, tumor cells infiltrate along myelinated fibers and disrupt normal cell structure [13]. It is not clear how the directionality of water diffusion and FA are affected by preserved fiber tracts, normal cell structure, and vigorous edema in peritumoral regions. Third, the present results do not apply to brain tumors other than glioblastoma, because the histologic structures of the other tumors differ from those of glioblastoma. For example, the FA value of gliomatosis cerebri with moderate cell density is equivalent to that of glioblastoma, because preservation of normal axons increases the extent of directionality of water diffusion [3]. Correlation of FA value with cell density and proliferation activity is required for each tumor using a study group limited to 1 type.

In conclusion, our findings suggested that the FA value of glioblastoma is determined at the very least by cell density and, consequently, correlates with proliferation activity, although the sample size of the present study was small. Measurement of FA value using DTI will most likely become an option for auxiliary examinations prior to surgery for glioblastoma.

Acknowledgments

This study was supported in part by a grant-in-aid for Advanced Medical Science Research from the Ministry of Science, Education, Sports and Culture, Japan.

References

[1] Bammer R, Augustin M, Strasser-Fuchs S, Seifert T, Kapeller P, Stollberger R, Ebner F, Hartung HP, Fazekas F. Magnetic resonance diffusion tensor imaging for characterizing diffuse and focal white matter abnormalities in multiple sclerosis. Magn Reson Med 2000; 44:583-91.

[2] Basser PJ, Pierpaoli C. Microstructural and physiological features of tissues elucidated by quantitative-diffusion-tensor MRI. J Magn Reson B 1996;111(3):209-19.

[3] Beppu T, Inoue T, Shibata Y, Kurose A, Arai H, Ogasawara K, Ogawa A, Nakamura S, Kabasawa H. Measurement of fractional anisotropy using diffusion tensor MRI in supratentorial astrocytic tumors. J Neurooncol 2003;63:109-16.

[4] Brunberg JA, Chenevert TL, McKeever PE, Ross DA, Junck LR, Muraszko KM, Dauser R, Pipe JG, Betley AT. In vivo MR determination of water diffusion coefficients and diffusion anisotropy: correlation with structural alteration in gliomas of the cerebral hemispheres. AJNR Am J Neuroradiol 1995;16:361-71.

[5] Castillo M, Smith JK, Kwock L, Wilber K. Apparent diffusion coefficients in the evaluation of high-grade cerebral gliomas. AJNR Am J Neuroradiol 2001;22(1):60-4.

[6] Chien D, Kwong KK, Gress DR, Buonanno FS, Buxton RB, Rosen BR. MR diffusion imaging of cerebral infarction in humans. AJNR Am J Neuroradiol 1992;13:1097-105.

[7] Ciccarelli O, Werring DJ, Wheeler-Kingshott CAM, Barker GJ, Parker GJM, Thompson AJ, Miller DH. Investigation of MS normal-appearing brain using diffusion tensor MRI with clinical correlations. Neurology 2001;56:926-33.

[8] Filippi M, Cercignani M, Inglese M, Horsfield MA, Comi G. Diffusion tensor magnetic resonance imaging in multiple sclerosis. Neurology 2001;56:304-11.

[9] Filippi CG, Edgar MA, Ulug AM, Prowda JC, Heier LA, Zimmerman RD. Appearance of meningiomas on diffusion-weighted images: correlating diffusion constants with histopathologic findings. AJNR Am J Neuroradiol 2001;22(1):65-72.

[10] Heesters MA, Koudstaal J, Go KG, Molenaar WM. Proliferation and apoptosis in long-term surviving low grade gliomas in relation to radiotherapy. J Neurooncol 2002;58:157-65.

[11] Hsu SM, Raine L, Fanger H. Use of avidin-biotin-peroxidase complex (ABC) in immunoperoxidase techniques: a comparison between ABC and unlabeled antibody (PAP) procedures. J Histochem Cytochem 1981;29:577-80.

[12] Karamitopoulou E, Perentes E, Diamantis I, Maraziotis T. Ki-67 immunoreactivity in human central nervous system tumors: a study with MIB 1 monoclonal antibody on archival material. Acta Neuropathol (Berl) 1994;87(1):47-54.

[13] Kleihues P, Cavenee WK. World Health Organization classification of tumours: pathology and genetics, tumours of the nervous system. Lyon: International Agency for Research on Cancer (IARC); 2000. p. 6-92.

[14] Kono K, Inoue Y, Nakayama K, Shakudo M, Morino M, Ohata K, Wakasa K, Yamada R. The role of diffusion-weighted imaging in patients with brain tumors. AJNR Am J Neuroradiol 2001;22(6): 1081-8.

[15] Krabbe K, Gideon P, Wagn P, Hansen U, Thomsen C, Madsen F. MR diffusion imaging of human intracranial tumours. Neuroradiology 1997;39(7):483-9.

[16] Melhem ER, Itoh R, Jones L, Barker PB. Diffusion tensor MR imaging of the brain: effect of diffusion weighting on trace and anisotropy measurements. AJNR Am J Neuroradiol 2000;21:1813-20.

[17] Pierpaoli C, Jezzard P, Basser PJ, Barnett A, Di Chiro G. Diffusion tensor MR imaging of the human brain. Radiology 1996;201:637-48.

[18] Pierpaoli C, Basser PJ. Toward a quantitative assessment of diffusion anisotropy. Magn Reson Med 1996;36(6):893-906.

[19] Schroder R, Feisel KD, Ernestus RI. Ki-67 labeling is correlated with the time to recurrence in primary glioblastomas. J Neurooncol 2002; 56:127-32.

[20] Sinha S, Bastin ME, Whittle IR, Wardlaw JM. Diffusion tensor MR imaging of high-grade cerebral gliomas. AJNR Am J Neuroradiol 2002;23(4):520-7.

[21] Sorensen AG, Buonanno FS, Gonzalez RG, Schwamm LH, Lev MH, Huang-Hellinger FR, Reese TG, Weisskoff RM, Davis TL, Suwanwela N, Can U, Moreira JA, Copen WA, Look RB, Finklestein SP, Rosen BR, Koroshetz WJ. Hyperacute stroke: evaluation with combined multisection diffusion-weighted and hemodynamically weighted echo-planar MR imaging. Radiology 1996;199(2):391-401.

[22] Sugahara T, Korogi Y, Kochi M, Ikushima I, Shigematu Y, Hirai T, Okuda T, Liang L, Ge Y, Komohara Y, Ushio Y, Takahashi M. Usefulness of diffusion-weighted MRI with echo-planar technique in the evaluation of cellularity in gliomas. J Magn Reson Imaging 1999;9:53-60.

[23] Tien RD, Felsberg GJ, Friedman H, Brown M, MacFall J. MR imaging of high-grade cerebral gliomas: value of diffusion-weighted echoplanar pulse sequences. AJR Am J Roentgenol 1994;162(3): 671-7.

[24] Tievsky AL, Ptak T, Farkas J. Investigation of apparent diffusion coefficient and diffusion tensor anisotropy in acute and chronic multiple sclerosis lesions. AJNR Am J Neuroradiol 1999;20:1491-9.

[25] Wakimoto H, Aoyagi M, Nakayama T, Nagashima G, Yamamoto S, Tamaki M, Hirakawa K. Prognostic significance of Ki-67 labeling indices obtained using MIB-1 monoclonal antibody in patients with supratentorial astrocytomas. Cancer 1996;77(2):373-80.

[26] Witwer BP, Moftakhar R, Hasan KM, Deshmukh P, Haughton V, Field A, Arfanakis K, Noyes J, Moritz CH, Meyerand ME, Rowley HA, Alexander AL, Badie B. Diffusion-tensor imaging of white matter tracts in patients with cerebral neoplasm. J Neurosurg 2002;97: 568-75.

[27] Yasargil MG. Microneurosurgery IV A [in 4 volumes]. Stuttgart/New York Verlag: Georg Thieme; 1993. p. 127 [for distribution in Japan: Nankodo Company Ltd Tokyo].

[28] Yoshiura T, Wu O, Zeheer A, Reese TG, Sorensen G. Highly diffusion-sensitized MRI of brain: dissociation of gray and white matter. Magn Reson Med 2001;45:734-40.

Commentary

In this interesting article, Beppu et al suggest that diffusion tensor imaging can be used to look at the disruption of fibers by an invasive tumor. This is a potentially important application of this novel technique to the analysis of brain tumors. At the Brigham and Women's Hospital, we have developed this technology primarily to assess to what degree low-grade tumors infiltrate rather than disrupt fibers. It has been an important tool for assessing the likelihood that surgery will cause new deficits in patients with these tumors.

The findings of Beppu et al are what we all might well believe—that glioblastomas are invasive tumors that significantly disrupt normal fiber tracts. Although the study has relatively few patients, the techniques are quite demanding and therefore worthwhile reading. This is a valuable addition to the literature of neurosurgical oncology to decide whether surgery should be done.

Peter M. Black, MD, PhD
Department of Neurosurgery
Children's Hospital
Boston, MA 02115, USA

J Neurosurg 100:1101–1106, 2004

Gradual recovery from dyslexia and related serial magnetoencephalographic changes in the lexicosemantic centers after resection of a mesial temporal astrocytoma

Case report

KYOUSUKE KAMADA, M.D., YUTAKA SAWAMURA, M.D., FUMIYA TAKEUCHI, PH.D., KIYOHIRO HOUKIN, M.D., HIDEAKI KAWAGUCHI, M.D., YOSHINOBU IWASAKI, M.D., AND SHINYA KURIKI, PH.D.

Department of Neurosurgery, Research Institute for Electronic Science, Department of Laboratory Medicine, Hokkaido University; and Department of Neurosurgery, Sapporo Medical College, Sapporo, Japan

✓ Letter-perception centers are not held in as high regard as motor- and language-related cortices during planning of neurosurgical procedures, and there have been no reports suggesting cortical reorganization of reading ability. The authors describe a patient with a left mesial temporal glioma in whom two letter-perception centers (the anterior portion of the left superior temporal gyrus and the left fusiform gyrus) were successfully localized before surgery by performing magnetoencephalography (MEG) during reading tasks. Control MEG examinations of 15 healthy volunteers were also performed to assist in a careful interpretation of patient results. Although a radical resection of the mesial temporal glioma, which involved the left fusiform gyrus, caused severe dyslexia, the patient's impaired reading skills improved gradually during a 1-year postoperative period. In the meantime, the spared left superior temporal gyrus displayed an overshot recovery of MEG responses. During the postoperative period there was no obvious recovery in MEG signals and no compensatory activity in the contralateral fusiform gyrus. This case demonstrates that lexicosemantic centers involved in the reading process can be noninvasively localized using MEG and that the results obtained are highly reliable for surgical planning. The results of the repeated MEG reflected sequentially the patient's recovery from dyslexia. This is the first report in which MEG studies have been shown to predict preoperatively the risk of dyslexia and demonstrate its serial physiological recovery.

KEY WORDS • dyslexia • glioma • mesial temporal lobe • functional recovery • magnetoencephalography

It has been generally accepted that resections performed in the language-dominant hemisphere must spare the classic frontal motor and temporal receptive language areas to avoid persistent aphasia. Most neurosurgeons have strictly followed this basic guideline, even in glioma surgery.

On the other hand, the cortical areas related to letter perception have not been well acknowledged. The semantic center of letter reading has not been seriously considered during surgical planning. Reading impairments such as dyslexia can be masked by coexistent major complications such as aphasia or dementia. Nevertheless, dyslexia essentially affects patients' intellectual life and work and is a subject that should be duly considered as a major complication.

Previous studies of lesions have demonstrated that the superior temporal and angular gyri in the dominant hemisphere contribute mainly to letter-reading processes.[5,6] Nobre, et al.,[11] found the site of lexicosemantic activity related to the reading process in the inferior temporal region, including the fusiform gyrus, by using subdural electrodes. Studies in healthy volunteers in which noninvasive functional imaging techniques such as PET and fMR imaging were performed have demonstrated that the inferior temporal area is activated by several reading tasks.[3,13,14] The functional dominance of the fusiform gyrus, however, remains unclear because most studies have demonstrated bilateral responses in reading processes.

Magnetoencephalography directly detects neuronal activity and provides a better time resolution than other noninvasive methods of mapping. In this report, an MEG investigation in which letter-reading tasks were performed preoperatively localized the lexicosemantic centers in a patient with a left mesial temporal glioma. After complete resection of the tumor, which involved the inferomesial temporal region in which the semantic-MEG dipoles were concentrated, the patient suffered from severe dyslexia. He gradually recovered within 1 year. We followed the patient's recovery by performing serial MEG, which reflected the severity of the dyslexia and the clinical usefulness of lexicosemantic MEG.

Abbreviations used in this paper: fMR = functional magnetic resonance; IQ = intelligence quotient; LORETA = low-resolution electromagnetic tomography; MEG = magnetoencephalography; PET = positron emission tomography; RMS = root mean square; SLTA = Standard Language Test for Aphasia; WAIS-R = Wechsler Adult Intelligence Test–Revised.

TABLE 1
*Results of the SLTA and lexicosemantic MEG investigations**

	SLTA Score (%)				MEG	
Timing	Reading	Writing	Speech	Verbal Comprehension	Mean Reaction Time (msec)†	Task Performance (%)
preop	100	100	100	100	800 ± 213	92.3
7 or 10 days‡	42	75	78	80	NT	NT
3 mos	80	88	90	90	1320 ± 379§	63.8
8 mos	90	92	97	98	1212 ± 305§	83.0

* NT = not tested.
† Mean ± standard deviation.
‡ Neuropsychological tests and the MEG study were performed 7 and 10 days postoperatively, respectively.
§ $p < 0.5$, Student t-test.

Case Report

History. This 34-year-old, right-handed man experienced transient amnesia for a few minutes in April 2001. Before the incident he had done well in his employment as an office worker. Neurological examination revealed no abnormality on the day after the episode, but T_1-weighted MR images revealed a large hypointense mass in the left mesial temporal region. The lesion appeared homogeneously hyperintense on T_2-weighted MR images and was not enhanced following a Gd–diethylenetriamine pentaacetic acid injection. The mass involved the hippocampus, uncus, amygdala, and parahippocampal and fusiform gyri, but not the superior or middle temporal gyri. These findings suggested that the mass was a low-grade astrocytoma originating from the mesial temporal lobe. No neurological deficit had appeared before treatment and thus our major concern was whether the brain area to be involved in surgery would still function postoperatively.

Examination. Preoperative neuropsychological examinations, including the SLTA (Japanese edition), WAIS-R, Miyake auditory–verbal memory test, and Benton Visual Retention Test detected no language deficits or memory disturbance. The SLTA is the standardized test battery most commonly used to evaluate Japanese patients with aphasia. The aphasia severity ratings (range 0, most severe–10, normal) are based on the 19 subscores of the SLTA, and these were used as a primary language measurement for this patient. The following six subscores of the SLTA were sequentially analyzed: reading aloud words; reading comprehension (in which the patient points out images of objects indicated by written words); dictation of letters; naming; auditory comprehension (ability to obey verbal commands); and sentence repetition. The patient could complete the tasks of the SLTA without difficulty and obtained full points for all the subscores. The verbal and performance IQs, determined using the WAIS-R, were 112 and 118, respectively. The patient's hand preference was predominantly right sided (+105 on the Edinburgh Handedness Inventory),[9] and an intracarotid sodium amobarbital test (Wada test) revealed a left-hemisphere dominance for language functions and a right-hemisphere dominance for memory. Lexicosemantic MEG, performed using a letter-reading task, localized two letter-perception centers (the anterior portion of the left superior temporal gyrus and the left fusiform gyrus), as described in detail later in this paper. Because this large low-grade glioma was thought to be life threatening, but curable by a complete resection, we proposed radical removal of the tumor involving the inferior temporal region, informing the patient of the risks of possible postsurgical neurological deficits. The patient accepted the treatment plan and gave his informed consent to participate in pre- and postoperative lexicosemantic examinations including MEG and neuropsychological tests.

Operation. The middle and inferior temporal gyri were exposed by a frontotemporal craniotomy. The brain tumor was found after a corticotomy, which encompassed a 4-cm anterior portion of the inferior temporal gyrus. Intraoperative observation disclosed tumor invasion into the inferior temporal gyrus, fusiform gyrus, amygdala, uncus, and hippocampus. The involved brain tissue was completely resected. The histopathological diagnosis was World Health Organization Grade II diffuse astrocytoma.

Postoperative Course. The patient awoke with severe dyslexia and a slight receptive aphasia. Auditory comprehension and repetition and naming capabilities were almost intact. Neurological and neuropsychological examinations were serially performed throughout an 8-month postoperative period. On the 7th postoperative day, the man still displayed severe reading and writing impairments (scores of 3 in reading aloud, 4 in reading comprehension, and 7 in letter dictation; Table 1) with a right upper homonymous quadrantanopia. Speech function and auditory comprehension were, however, relatively preserved. The man's verbal IQ (WAIS-R) was 88, which was lower than preoperatively despite the fact that he retained a normal performance IQ (116).

Three months after surgery, the impairments had improved, but he still had difficulty in reading and exhibited phonemic paralexia (scores of 6 in reading aloud and 8 in reading comprehension). It is noteworthy that he could point out objects correctly with a finger, even though he could not read aloud the names of written objects (understanding without phonology) (Table 1). Eight months after surgery, the patient's reading impairment had remarkably improved (scores of 8.5 in reading aloud and 9 in reading comprehension) and he became able to read newspapers with some effort. His verbal IQ (103) was much improved, but did not reach his preoperative level.

The Miyake auditory–verbal memory test and the Benton Visual Retention Test did not show any deterioration in the patient's short-term memory and, clinically, he displayed little memory disturbance following the operation. He returned to his office work, but still acknowledged lingering reading difficulties.

Summary of Tests and Findings

Lexicosemantic MEG Studies

The MEG signals were recorded using a 204-channel biomagnetometer (VectorView; Neuromag, Helsinki, Finland) in a magnetically shielded room. Serial MEG studies were performed before the operation and 10 days, 3 months, and 8 months after surgery. Despite the fact that the patient's reading comprehension skills generally improved throughout the postoperative period, the postoperative MEG findings were compared with the preoperative MEG findings. We acquired two data sets for each task to confirm stable and consistent MEG responses. In particular, we performed the preoperative MEG investigations on two different days (7 and 3 days before surgery) and also performed control examinations in 15 strongly right-handed volunteers who had experienced no adverse cerebral events or neurological deficits.

One hundred fifty words were visually presented with a 300-msec exposure time and interstimulus intervals ranging between 2800 and 3200 msec during the MEG recordings. Each word was a noun that consisted of three kana letters (Japanese phonetic symbols that were presented, centered at a 4° visual angle). The patient and volunteers were asked to categorize the presented word as abstract or concrete by pushing buttons with the index or middle finger, respectively (kana reading). To identify the lexicosemantic response specific to the kana-reading task, we presented 150 pairs of Arabic letters and asked the patient and volunteers to decide whether each pair had the same letters or different ones (figure discrimination). All volunteers and the patient received instructions and were allowed brief practice sessions before the measurement.

Each epoch consisted of a 500-msec prestimulus baseline and a 1500-msec analysis period following stimulus delivery. One hundred fifty epochs of magnetic signals were averaged and digitally filtered between 0.5 and 40 Hz. Significant deflections of neuromagnetic fields were visually identified on the basis of RMS fields containing more than 10 sensors in the frontotemporal or temporooccipital regions. Locations and dipole moments of equivalent current dipoles were calculated every 2 msec for each selected time period by using the single equivalent dipole model. Only dipoles with a correlation value greater than 0.9 between measured and calculated field distributions were accepted. To confirm the calculated results, the same MEG time periods were analyzed using one of the following: current-density maps or LORETA (Curry; Neuroscan Labs, Sterling, VA).

The estimated dipoles were converted into three-dimensional MR images by identifying external anatomical fiduciary markers (nasion and left and right preauricular points).

Serial Changes in the Lexicosemantic MEG Studies

Preoperative MEG Findings. The patient and healthy volunteers could easily complete both tasks after a brief practice period. The mean reaction time and the percentage of successful task performance of the patient were approximately 800 msec and 92.3%, respectively, which were within normal range (Table 1). Figure 1 depicts the RMS fields of the preoperative MEG study *(thick black line)* with the kana-reading task in the bilateral frontotemporal and temporooccipital regions. Late deflections peaking at approximately 350 msec were observed in both of the left frontotemporal and temporooccipital regions. In the contralateral hemisphere (right frontotemporal and temporooccipital regions), however, early and short-duration RMS peaks were recorded approximately 250 msec after the stimulation. In all 15 healthy volunteers, the late deflections were predominantly observed in the left frontotemporal region rather than in the right hemisphere. On the other hand, in the temporooccipital region there was no late response in five volunteers (33.3%), left-side dominance in seven (46.7%), and right-side dominance in three (20%).

The figure discrimination task evoked only early deflections (within 300 msec) in both hemispheres with no later activation in the patient or any volunteer; therefore, we considered that the later responses in the left hemisphere might be strongly related to the lexicosemantic processes in letter perception on the basis of our preliminary results and previous reports.[9]

Figure 2 demonstrates the representative MEG sources in two healthy volunteers. The left hemispheric responses were mainly localized in the superior, middle temporal, and supramarginal gyri (mean number of dipoles 122.4). In contrast, in the right hemisphere there were far fewer numbers of estimated dipoles (mean number of dipoles 32.4). Concerning the location of the temporooccipital dipoles, it was not common for the left inferior temporal region to have predominantly more dipoles than the right side. There was no consistent dominance of temporooccipital dipoles between the hemispheres (Fig. 2).

In the patient, the estimated dipoles of the left frontotemporal response were mainly concentrated in the anterior portion of the left superior and middle temporal gyri (38 dipoles) (Fig. 3A and B). Additionally, 102 dipoles of the left temporooccipital responses were densely concentrated adjacent to the posterior border of the tumor in the fusiform gyrus (Fig. 3C and D), which was relatively strong compared with the control data. The right frontotemporal and temporooccipital responses of the patient were observed in the right supramarginal gyrus and in the fusiform gyrus, respectively. The 24 right-hemisphere dipoles did not reach even one third of that of the left hemisphere, indicating left-side dominance for the reading process in this patient. It was notable that all 102 dipoles in the left hemisphere were mainly located in the fusiform gyrus where the tumor invaded. The LORETA analysis demonstrated two clusters of stronger sources in the anterior portion of the left superior temporal gyrus and the left fusiform, as did the single equivalent dipole model. We reexamined the patient 4 days after the first examination to confirm that the lexicosemantic MEG should reveal the consistent results for preoperative functional mapping. The second MEG examination demonstrated that the left fusiform gyrus was extremely active with the letter-reading task, just as the first examination had.

Postoperative MEG Findings. On the 10th day after surgery, the patient could not complete the reading task due to severe dyslexia. He was, therefore, asked to look passively at the presented letters. The most significant change on the MEG study was that no significant responses were detected in the left hemisphere (Fig. 1).

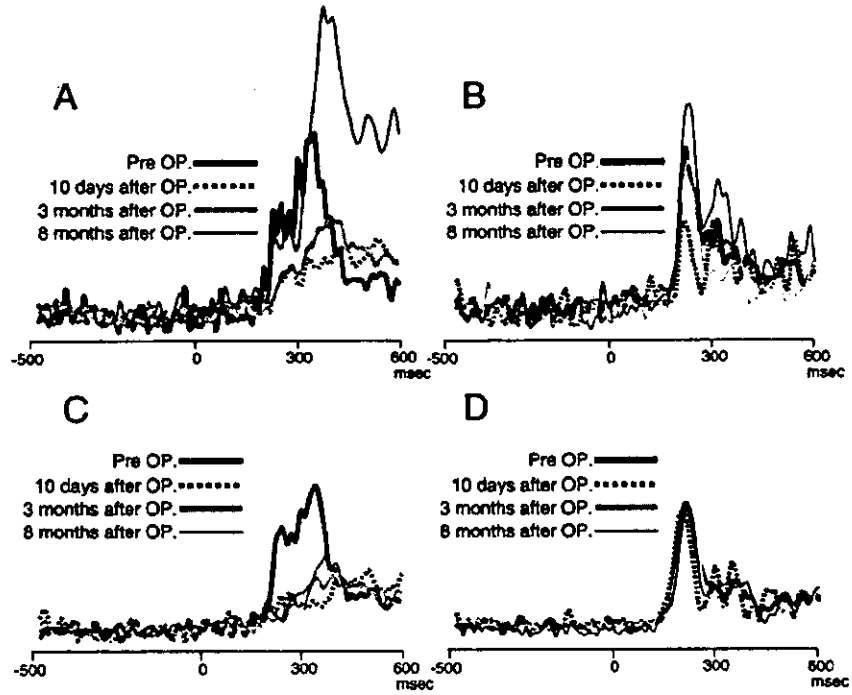

FIG. 1. Four RMS profiles of lexicosemantic MEG responses during the letter-reading task from the left (A) and right (B) frontotemporal regions and from the left (C) and right (D) temporooccipital regions. The left frontotemporal responses, which peaked at 400 msec, are markedly decreased in amplitude and the left temporooccipital responses became silent after the resection. Note that the RMS profile from the left frontotemporal region becomes approximately 1.5 times higher in amplitude 8 months after surgery, despite no changes in the bilateral temporooccipital regions.

Three months after surgery, the patient's reading skills had improved and he could slowly read kana character by character. His mean reaction time and rate of success were approximately 1320 msec and 63.8%, respectively, which remained worse than his performance preoperatively. Although small RMS deflections appeared in the left frontotemporal region, peaking at approximately 420 msec (later than the preoperative response), these responses were too small in amplitude to localize. There was no obvious deflection in the left temporooccipital region. In contrast to the left hemisphere, the RMS profiles detected in the right frontotemporal region were almost identical to the preoperative MEG studies.

Eight months after surgery, the patient had recovered notably from the dyslexia and could perform the reading task with some effort. His mean reaction time and rate of success were further improved. It is noteworthy that the amplitudes of the left frontotemporal responses were more than 1.5 times higher than those of the preoperative responses. Estimated dipoles of the left frontotemporal response were mainly concentrated in the anterior portion of the superior and middle temporal gyri (78 dipoles) (Fig. 4) and showed 56.4 nAm of the mean dipole moment, which was 1.5 times stronger than that of the preoperative response (36.2 nAm). The peak latency periods of the left frontotemporal responses, however, were still later than those measured preoperatively (at ~ 420 msec). The activities of the left temporooccipital region remained quiescent. The right frontotemporal region revealed a sharp RMS deflection with slightly high amplitudes, peaking at 250 msec after the stimuli. The right temporooccipital responses had been consistently peaking at approximately 250 msec with similar RMS amplitudes throughout the serial MEG investigations. The right hemisphere had 37 dipoles in the frontotemporal and temporooccipital regions.

Discussion

The radical resection of the mesial temporal glioma injured the left fusiform gyrus, where the lexicosemantic MEG dipoles were concentrated, and, as a result, caused severe dyslexia. The patient's impaired reading skills, however, were generally improved a year later. In the meantime the spared left frontotemporal region, which used to be one of the semantic centers, produced an overshot recovery of MEG responses. This finding indicates that MEG provides a noninvasive method of identifying and visualizing the lexicosemantic centers used in the reading process. It is a matter of course that the preoperative identification of eloquent cortices related to higher brain functions is beneficial for neurosurgical planning. Furthermore, it is scientifically important that the sequential recovery of MEG signals on repeated studies be observed along with the patient's clinical recovery from dyslexia.

Although it is well known that right-handed patients with left inferior temporal lesions suffer from impaired reading skills, we empirically know that dyslexia may not appear in 100% of these patients and that if it does, it sometimes is improved later. Researchers who have performed PET studies in healthy volunteers have reported that visually presented letters activate the bilateral superior temporal and posterior inferior temporal regions as well as the Broca area.[15,16]

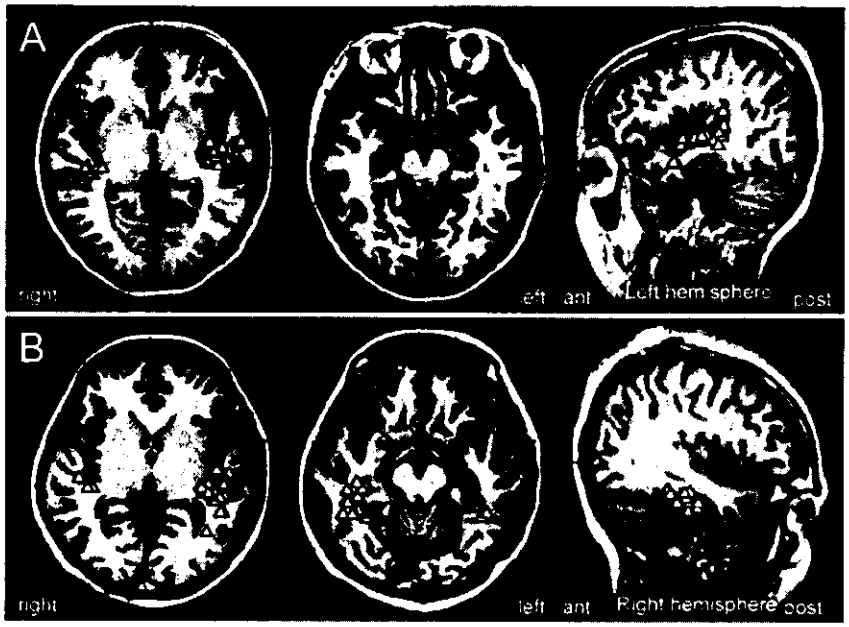

FIG. 2. Lexicosemantic MEG dipole distributions in two healthy volunteers (Volunteers A and B). Estimated dipoles of late deflections in the frontotemporal regions are predominantly concentrated in the left hemisphere (107 dipoles in Volunteer A and 90 in Volunteer B) compared with the right side (42 and 22 dipoles, respectively). The temporooccipital regions exhibit no late response (Volunteer A) and a right-side–dominant dipole distribution (45 dipoles in the right and four dipoles in the left hemispheres of Volunteer B).

Measurements of evoked potentials in patients with epilepsy have demonstrated responses at approximately 200 msec (N200) on the cortices of the bilateral temporal base, including the fusiform gyrus, after letter presentation.[1,10,11] The sole function of the fusiform gyrus can barely be investigated using cortical stimulation, fMR imaging or PET scanning, because of its anatomical characteristics (small size and deep location) and the surrounding vascular structures (the vein of Labbé and the basal veins of Rosenthal). The functional role and dominance of the fusiform gyrus, therefore, remain obscure.

Authors of recent MEG studies performed in healthy volunteers have found lexicosemantic activity in the fusiform gyrus and the left superior temporal gyrus at approximately 200 (early) and 400 (late) msec following letter presentation, respectively.[7,8] Authors of these studies have emphasized that the fusiform gyrus as well as the left superior temporal gyrus may principally contribute to reading processes. Although the temporooccipital regions of normal controls exhibited various dipole distributions, such as left-side dominance (46.7%), right-side dominance (20%), and no response (33.3%) in our preliminary study, strong activation was especially demonstrated in the left fusiform gyrus in our patient. On the basis of these results, the fusiform gyrus of the dominant hemisphere plays an important role for reading processes, but the functional dominance of this structure should be carefully investigated for each patient.

It is noteworthy that the patient's dyslexia remarkably improved until 8 months following resection of the fusiform gyrus in his dominant hemisphere. Previous PET and fMRI imaging studies have indicated a possibility of cortical reorganization in patients who display dramatic recoveries of motor functions.[2,4] These studies have demonstrated activations not only in the contralateral cortex, but also in the ipsilateral sensorimotor cortex and in other cortical regions, indicating the involvement of a widespread network in the recovery process.[2] In our case, the left temporooccipital region became silent on MEG following resec-

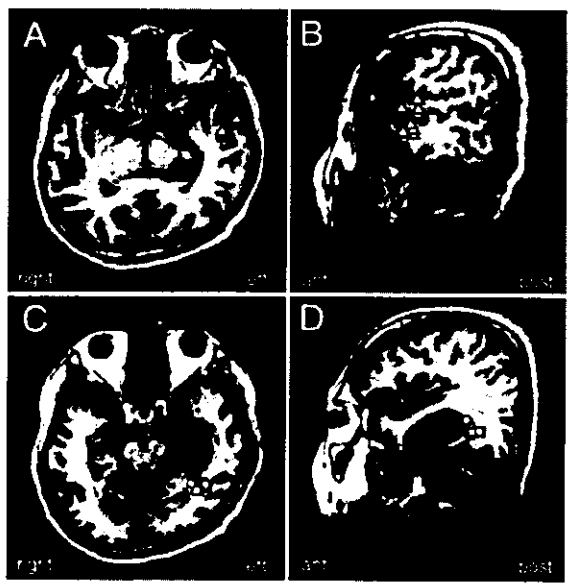

FIG. 3. Lexicosemantic MEG dipole locations in the left frontotemporal (A and B) and left temporooccipital regions (C and D) before surgery. The dipoles are concentrated in the anterior portion of the superior and middle temporal gyri *(white triangles)* and in the fusiform gyrus *(white squares)*, which contains the tumor.

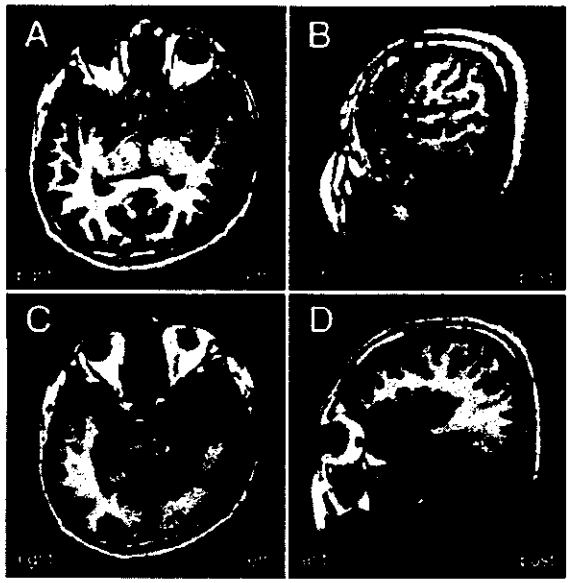

FIG. 4. Lexicosemantic MEG dipole locations in the left frontotemporal (A and B) and temporooccipital regions (C and D) 8 months after surgery. The left frontotemporal dipoles are located in the anterior portion of the superior and middle temporal gyri; however, there are no dipoles in the left temporooccipital region, including the fusiform gyrus.

tion, whereas the responses of the contralateral homologous (right) temporooccipital region constantly maintained the same RMS profiles. The left frontotemporal region showed a marked recovery in MEG amplitude, but the peak latency period did not completely return to its preoperative state. Although we observed no compensatory activity or reorganization in the ipsilateral temporooccipital region, the responses of the left frontotemporal region at 8 months after surgery became 1.5 times higher in amplitude than those before surgery. The patient experienced difficulty in reading letters after surgery and thus required more concentration to perform the reading task. One should consider, at least in part, that the spared left frontotemporal region might have contributed to the patient's recovery from dyslexia.

Our single equivalent dipole model provided a similar result to those of previous reports[7,8,15,17] and is helpful for understanding the process of language perception. Nevertheless, it is critical to consider the responsibility of multiple dipoles existing in the bilateral fusiform gyrus or in other regions, which may provide additional supplementary functions in the reading process. The LORETA is one of the currently available density maps that can potentially be used to analyze multiple sources in the electro- and magnetophysiological fields.[9] It can separately localize two or three active sources with different time courses, which the single dipole model fails to localize. Because LORETA and the single dipole approach yield the same results, the source localization of this study became more reliable. Furthermore, the resection of the fusiform gyrus that produced the active sources resulted in severe dyslexia.

Although preliminary, this case study demonstrates that MEG performed using the kana reading task can readily identify the semantic magnetic responses and provide a noninvasive means for analyzing functional brain structures relating to letter perception. To our knowledge, this is the first report in which a method has been introduced that can be used to predict a risk for postoperative dyslexia and monitor functional recovery from the symptom. This technique can be applied to analyze other semantic processes and will be a useful tool in the elucidation of the pathophysiology of aphasia, dysphasia, and dyslexia.

References

1. Allison T, McCarthy G, Nobre A, et al: Human extrastriate visual cortex and the perception of faces, words, numbers, and colors. **Cereb Cortex 4:**544–554, 1994
2. Chollet F, DiPiero V, Wise RJS, et al: The functional anatomy of motor recovery after stroke in humans: a study with positron emission tomography. **Ann Neurol 29:**63–71, 1991
3. Cohen L, Lehericy S, Chochon F, et al: Language-specific tuning of visual cortex? Functional properties of the Visual Word Form Area. **Brain 125:**1054–1069, 2002
4. Feydy A, Carlier R, Roby-Brami A, et al: Longitudinal study of motor recovery after stroke: recruitment and focusing of brain activation. **Stroke 33:**1610–1617, 2002
5. Geschwind N: The organization of language and the brain. **Science 170:**940–944, 1970
6. Iwata M: Neural mechanism of reading and writing in the Japanese language. **Funct Neurol 1:**43–52, 1986
7. Kamada K, Kober H, Saguer M, et al: Responses to silent Kanji reading of the native Japanese and German in task subtraction magnetoencephalography. **Brain Res Cogn Brain Res 7:**89–98, 1998
8. Kuriki S, Hirata Y, Fujimaki N, et al: Magnetoencephalographic study on the cerebral neural activities related to the processing of visually presented characters. **Brain Res Cogn Brain Res 4:** 185–199, 1996
9. Mulert C, Gallinat J, Pascual-Marqui R, et al: Reduced event-related current density in the anterior cingulate cortex in schizophrenia. **Neuroimage 13:**589–600, 2001
10. Nobre AC, McCarthy G: Language-related ERPs: scalp distributions and modulation by word type and semantic priming. **J Cogn Neurosci 6:**233–255, 1994
11. Nobre C, Allison T, McCarthy G: Word recognition in the human inferior temporal lobe. **Nature 372:**260–263, 1994
12. Oldfield RC: The assessment and analysis of handedness: the Edinburgh inventory. **Neuropsychologia 9:**97–113, 1971
13. Petersen SE, Fox PT, Posner MI, et al: Positron emission tomographic studies of the cortical anatomy of single-word processing. **Nature 331:**585–589, 1988
14. Sakurai Y, Momose T, Iwata M, et al: Semantic process in kana word reading: activation studies with positron emission tomography. **NeuroReport 4:**327–330, 1993
15. Salmelin R, Service E, Kiesila P, et al: Impaired visual word processing in dyslexia revealed with magnetoencephalography. **Ann Neurol 40:**157–162, 1996
16. Simos PG, Breier JI, Fletcher JM, et al: Brain activation profiles in dyslexic children during non-word reading: a magnetic source imaging study. **Neurosci Lett 290:**61–65, 2000

Manuscript received December 12, 2002.
Accepted in final form February 9, 2004.

Address reprint requests to: Kyousuke Kamada, M.D., Department of Neurosurgery, Graduate School of Medicine, University of Tokyo, 7-3-1 Hongo, Bunkyo-ku, Tokyo, 113-8655, Japan. email: kamady-k@umin.ac.jp.

Midkine promoter-based conditionally replicative adenovirus for malignant glioma therapy

SHOHEI KOHNO[1], KOU NAKAGAWA[1], KATSUYUKI HAMADA[2], HIRONOBU HARADA[1], KENSHI YAMASAKI[3], KOJI HASHIMOTO[3], MASATOSHI TAGAWA[4], SHIGEYUKI NAGATO[1], KOJI FURUKAWA[1] and TAKANORI OHNISHI[1]

Departments of [1]Neurosurgery, [2]Obstetrics and Gynecology, and [3]Dermatology, Ehime University School of Medicine, Ehime 791-0295; [4]Division of Pathology, Chiba Cancer Center Research Institute, Chiba 260-8717, Japan

Received December 22, 2003; Accepted February 12, 2004

Abstract. Little is known concerning promoters or gene therapy specific for malignant glioma. To explore the potential use of *midkine* promoter in gene therapy for malignant glioma, we constructed a *midkine* promoter-based conditionally replicating adenovirus (Ad-*MK*). *Midkine* was overexpressed in malignant glioma tissues but *cyclooxygenase-2* was not. The *midkine* promoter activity of the 600-bp fragment was 2 orders of magnitude higher in midkine-positive glioma cells than in midkine-negative primary normal brain cells. Ad-*MK* showed strong oncolytic effects in midkine-positive glioma cells but did not exhibit cytotoxicity in midkine-negative primary normal brain cells. The cell-killing effect was evident in E3-intact Ad-*MK* more than in E3-deleted Ad-*MK*. In an animal experiment, Ad-*MK* completely eradicated midkine-positive glioma xenografts. These findings indicate that *midkine* promoter-based conditionally replicative adenovirus might be a promising new modality of gene therapy for malignant glioma.

Introduction

Malignant glioma is characterized by rapidly growing and aggressively invasive neoplasm. Due to the lack of an effective treatment, the median survival associated with this diagnosis continues to be around 1 year (1), suggesting a pressing need for novel therapeutic strategy. Gene therapy has shown promise as a new approach for this malignancy, but the results of clinical trials with replication-deficient viral vectors and suicide gene therapy have been unsatisfactory with regard to therapeutic outcome (2). The main reason for these disappointing results is related to the limited spread of the vectors in the tumor mass. The new therapeutic modality provided by oncolytic virotherapy with conditionally replicative adenovirus (CRAd) is expected to advance the treatment of malignant glioma. The strategy is replacement of adenovirus promoters with tumor-specific promoters to control the expression of viral genes essential for replication. The tumor-specific promoters allow the expression of viral genes preferentially in cancer cells, so that the virus only replicates in and kills those cells. Tumor-specific promoters such as *α-fetoprotein*, *prostate-specific antigen*, *MUC1* and *cyclooxygenase-2* (*cox-2*) have been widely used experimentally to drive viral genes expression (3). However, an appropriate promoter for malignant glioma has not yet been identified. We are interested in the gene encoding midkine (MK), because it has been reported that MK expression closely correlates to carcinogenesis (4). MK is a heparin-binding growth factor identified as a product of a retinoic acid-responsive gene, and promotes growth, survival, migration and other activities of various cells. Overexpression of MK has been observed in several types of malignant neoplasms such as gastrointestinal cancer, ovarian cancer and breast cancer (5,6). It has also been reported that MK expression is elevated in malignant glioma, but not in normal brain tissue (7). These findings indicate that MK promoter might be a potential candidate for oncolytic gene therapy of malignant glioma.

In the present study, we examined the potency of *MK* promoter in a tumor-specific promoter-based replicative adenovirus constructed for oncolytic gene therapy of malignant glioma. First, we determined the MK expression levels in human glioma and normal brain tissues. Subsequently, we evaluated the *in vitro* and *in vivo* antitumor effect of CRAd in which expression of the *E1A* gene is driven by the *MK* promoter.

Correspondence to: Dr Shohei Kohno, Department of Neurosurgery, Ehime University School of Medicine, Shitsukawa, Shigenobu, Onsen-gun, Ehime 791-0295, Japan
E-mail: kouno@m.ehime-u.ac.jp

Key words: midkine, cyclooxygenase-2, CRAd, glioma, gene therapy

Materials and methods

Surgical specimens, cell lines and cell culture. Human specimens were surgically obtained from 12 glioblastomas (WHO grade IV), 4 anaplastic astrocytomas (WHO grade III), 3 diffuse astrocytomas (WHO grade II) and 5 normal brain tissues. Malignant glioma was defined as including glioblastoma and anaplastic astrocytoma. Primary normal brain cells were established in our laboratory. The human malignant

glioma cell line U87MG was obtained from the American Type Culture Collection (Manassas, VA); U251MG and U373MG were generously provided by Dr N. Arita (Hyogo College of Medicine, Hyogo, Japan); and LN319 was generously provided by Dr M. Tada (Hokkaido University School of Medicine, Sapporo, Japan). Cells were maintained in DMEM with 10% heat-inactivated fetal bovine serum. Cells were cultured at 37°C in a humidified atmosphere containing 5% CO_2.

Real-time quantitative RT-PCR. RNA samples (100 ng) were used in reverse transcription and real-time PCR for RNA expression studies. The reaction was carried out with the ABI PRISM 7700 sequence detection system (Applied Biosystems, Foster City, CA) in a total volume of 50 µl that contained TaqMan one-step RT-PCR master-mix (Applied Biosystems), 0.3 µM of each forward and reverse primer, and 0.21 µM of TaqMan probe. The forward and reverse primer and TaqMan probe were, respectively, 5'-GCGCGCTACAA TGCTCAGT-3', 5'-TGGCTTTGGCCTTTGCTTT-3' and 5'-CAGGAGACCATCCGCGTCACCAA-3' for *MK*, and 5'-GGTTGCTGGTGGTAGGAATGTT-3', 5'-CATAAAGCGT TTGCGGTACTCA-3' and 5'-CCGCAGTACAGAAAGTAT CACAGGCTTC CA-3' for *cox-2*. The reaction was performed with the following thermal cycling method: 30 min at 48°C for reverse transcription, 5 min at 95°C for AmpliTaq Gold activation, 15 sec at 95°C and 60 sec at 60°C for 40 cycles. *GAPDH* was chosen as a housekeeping gene to be tested as an endogenous control.

Western blot analysis. Cell lysate protein (10 µg) from each sample was subjected to 13.5% SDS-Tris glycerine gel electrophoresis and was then transferred to a polyvinylidene difluoride membrane (Bio-Rad Laboratories, Hercules, CA). Membranes were incubated with primary antibodies, rabbit anti-human MK monoclonal antibody generously provided by Dr H. Shimada (Chiba University Graduation School of Medicine, Chiba, Japan), rabbit anti-adenovirus-2 E1A polyclonal antibodies (Santa Cruz Biotechnology, Santa Cruz, CA) and human anti-ß-actin monoclonal antibody (Sigma-Aldrich Fine Chemical, St. Louis, MO). Membranes were also incubated with secondary antibodies, horseradish peroxidase-conjugated sheep anti-rabbit IgG (Dako, Glostrup, Denmark) and horseradish peroxidase-conjugated sheep antimouse IgG (Amersham, Piscataway, NJ).

Assay for MK promoter activity. The *MK* promoter of 600 bp (-562/33) or 2300 bp (-2285/33) in length, was cloned into the pGL3-basic vector (Promega, Madison, WI), which contained the firefly luciferase gene. Both DNA fragments were transfected into target cells with DOTAP Liposomal Transfection Reagent (Roche Molecular Biochemicals, Mannheim, Germany). Dual luciferase assays were performed according to the manufacturer's protocol (Promega). Luciferase activity in each plasmid was evaluated as the ratio to activity in the control plasmid (pGL3-SV40) driven by the *SV40* enhancer/promoter.

Construction of the adenovirus vector. The replication-competent Ad-*MK* including the adenoviral *E1A* region under the control of human *MK* promoter containing 600 bp or 2300 bp of the 5'-flanking region of the human *MK* gene was constructed. The pXC1 plasmid has adenovirus 5 sequences from 22 to 5790 bp containing the *E1* gene (Microbix Biosystems Inc., Toronto, Ontario, Canada). The 492-552 bp region of pXC1 was deleted to obtain pXC1-491. The *MK* promoter was ligated to pXC1-491 plasmid to obtain pXC1-MK. To construct the Ad-*MK*, homologous recombination was performed between pXC1-MK plasmid and the right hand side of pBHGE3 adenovirus DNA with the *E3* region and pBHG10 adenovirus DNA without the *E3* region in 293 cells by standard techniques (8). Wild-type adenovirus (Ad-*Wild*) and the *E1*-deleted AdCMV-*LacZ* virus were constructed as previously described (9). All of the viruses were purified with double cesium chloride gradients using standard method. Serial dilutions of viruses were plated on 293 cells for plaque assay, and the titer was expressed as plaque forming unit (pfu)/ml (multiplicity of infection, m.o.i.).

Cell count assay. A total of 3000 cells were plated in 12-well plates, and after 24 h, were infected with Ad-*MK600*, Ad-*MK2300*, Ad-*Wild* or AdCMV-*LacZ* viral control. Culture medium alone was used as a mock-infection control. Ten days after infection, IC_{50} was determined by counting the number of viable cells after staining with Trypan-blue.

Animal experiment. Nude mice 5-6 weeks of age were purchased from Charles River Laboratories (Tsukuba, Japan). Ten million each of U87MG and U373MG cells were inoculated s.c. into the flanks of mice in 200 µl of DMEM. The tumor growth was assessed by measuring bidimensional diameters every 3 days with calipers. The tumor volume was determined by using the simplified formula of rotational ellipse (1 x width^3 x 0.5). When the tumor reached a volume of approximately 100 mm^3, animals were randomly assigned to treatment groups. Animals were treated with a single intratumoral injection of adenovirus at $1x10^9$ pfu suspended in 100 µl of PBS. Each treatment group consisted of 5 animals.

Results

MK and Cox-2 gene expression in glioma tissues and cell lines. To measure the mRNA levels of the *MK* and *cox-2* gene, we performed real-time quantitative RT-PCR. We demonstrated the mRNA expression level of the *MK* and *cox-2* gene of each sample relative to that of *GAPDH* (Fig. 1). As shown in Table I, *MK* mRNA expression of malignant glioma tissues (glioblastoma and anaplastic astrocytoma) was 12 times that of diffuse astrocytoma ($P<0.05$, unpaired t-test) and 40 times that of normal brain tissues ($P<0.01$, unpaired t-test). However, *cox-2* gene expression did not significantly differ among the glioma samples and normal brain tissues. In diffuse astrocytomas and normal brain tissues, there was not significant difference between *MK* and *cox-2* mRNA expression. However, in malignant glioma tissues, mRNA expression of *MK* was 4 times that of *cox-2* ($P<0.01$, paired t-test).

To determine MK gene and protein expression in human glioma cell lines and primary normal brain cells, we performed real-time quantitative RT-PCR and Western blot analysis. The microscopic observation revealed that primary normal brain cells mainly consisted of glial cells. We determined the

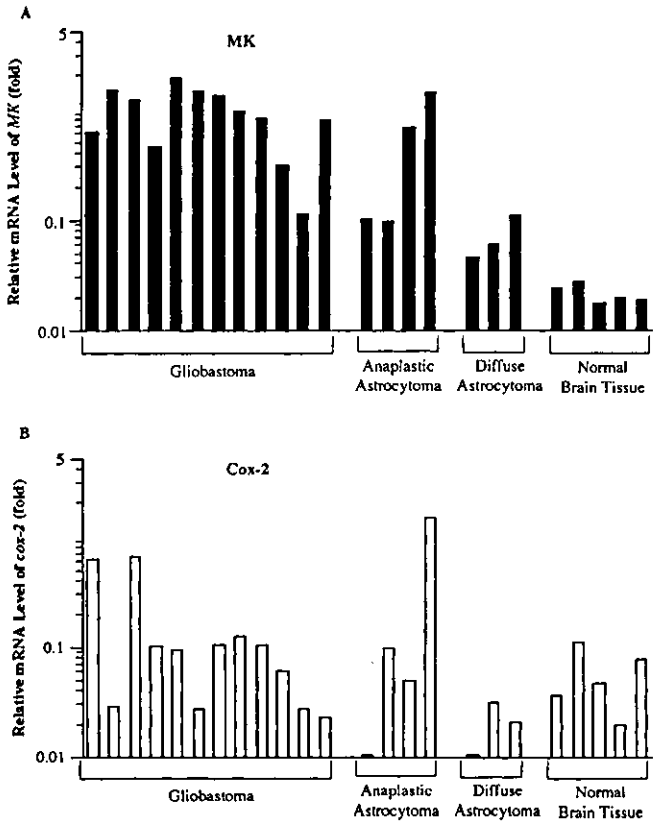

Figure 1. Expression of human *MK* and *cox-2* mRNA in glioma and normal brain tissues. Real-time quantitative RT-PCR was carried out to detect (A) *MK* or (B) *cox-2* mRNA expression in 12 glioblastomas, 4 anaplastic astrocytomas, 3 diffuse astrocytomas and 5 normal brain tissues.

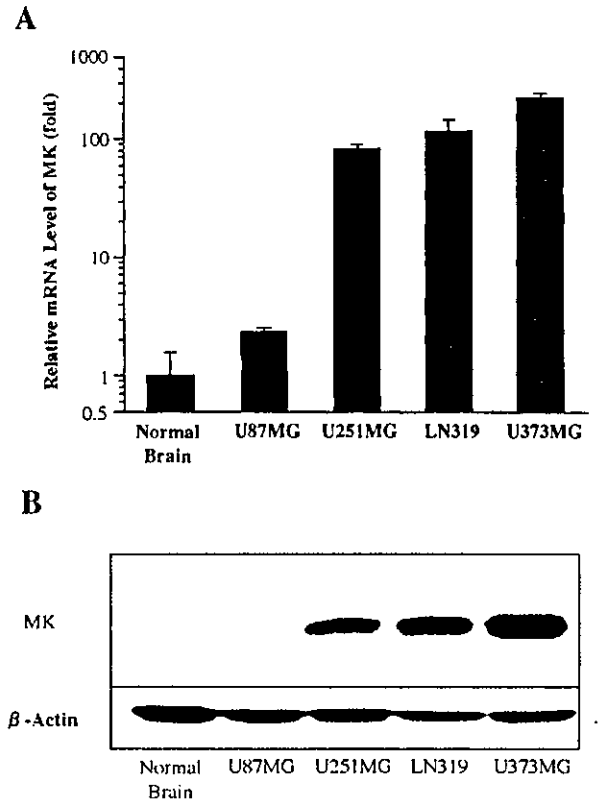

Figure 2. Expression of human MK. (A), *MK* mRNA expression of the glioma cell lines (U87MG, U251MG, LN319 and U373MG) and primary normal brain cells. The expression levels were determined by real-time quantitative RT-PCR. Bars, means ± SD; (B), Western blot analysis used to assay MK protein expression in the glioma and primary normal brain cells. Top panel shows the MK protein (16 kDa), and the ß-actin control is shown in the bottom panel.

Table I. Midkine and cox-2 expression in human glioma.

Tissue specimens	(n)	Midkine mRNA[a]	Cox-2 mRNA[a]
Malignant glioma (Glioblastoma + Anaplastic astrocytoma)	16	0.8585±0.544	0.2258±0.378
Diffuse astrocytoma	3	0.0722±0.028	0.0210±0.008
Normal brain tissue	5	0.0214±0.004	0.0578±0.032

[a]All values are expressed as the mean ± SD

mRNA expression level of the *MK* gene of each sample relative to that of primary normal brain cells after adjusting all samples for *GAPDH* gene expression. The mean value of *MK* mRNA of U251MG, LN319 and U373MG was 60 times that of U87MG (P<0.001, unpaired t-test) and 142 times that of primary normal brain cells (P<0.001, unpaired t-test; Fig. 2A). U251MG, LN319 and U373MG cells strongly expressed MK protein, whereas primary normal brain cells and U87MG did not (Fig. 2B). Therefore, we proceeded with subsequent experiments using U251MG, LN319 and U373MG as MK-positive cells, and U87MG and primary normal brain cells as MK-negative cells.

Transcriptional activity of MK promoter in glioma cell lines and primary normal brain cells. To compare the transcriptional activity of human *MK* promoter between MK-positive and negative cells, *MK* promoter activity was estimated with *SV40* promoter activity designated as 1 (Fig. 3). The promoter activity of the 600-bp fragment of the *MK* gene positively correlated with expression levels of *MK* mRNA (r=0.9; P<0.005, Pearson's correlation coefficient) and MK protein (r=0.9; P<0.005, Pearson's correlation coefficient). The transcriptional activity of the 600-bp fragment of the *MK* promoter in MK-positive glioma cells was 105 times that in primary normal brain cells (P<0.05, unpaired t-test) and 26 times that in U87MG (P<0.05, unpaired t-test). Moreover, transcriptional activity of pGL3-MK600 was 1.5 times that of pGL3-MK2300 in MK-positive cells (P<0.05, paired t-test), suggesting the presence of a negative regulatory element in the region from -2285 to -562 bp.

Selectivity of Ad-MK to adenovirus E1A expression in glioma cells. To confirm the activity and selectivity of Ad-*MK* on E1A